Published in final edited form as:
Apoptosis. 2009 July ; 14(7): 849–863. doi:10.1007/s10495-009-0356-4.

Selective apoptosis induction by the cancer chemopreventive agent *N*-(4-hydroxyphenyl)retinamide is achieved by modulating mitochondrial bioenergetics in premalignant and malignant human prostate epithelial cells

Numsen Hail Jr., **Ping Chen**, and **Jadwiga J. Kepa**
Department of Pharmaceutical Sciences, University of Colorado Denver School of Pharmacy, C238-P15 Research 2, 12700 E. 19th Avenue, Room 3008, Aurora, CO 80045, USA

Abstract

Prostate tumorigenesis is coupled with an early metabolic switch in transformed prostate epithelial cells that effectively increases their mitochondrial bioenergetic capacity. The synthetic retinoid *N*-(4-hydroxyphenyl)retinamide (4HPR) inhibits prostate cancer development in vivo, and triggers reactive oxygen species (ROS)-dependent prostate cancer cell apoptosis in vitro. The possibility that 4HPR-induced ROS production is associated with mitochondrial bioenergetics and required for apoptosis induction in transformed prostate epithelial cells in vitro would advocate a prospective mechanistic basis for 4HPR-mediated prostate cancer chemoprevention in vivo. We investigated this tenet by comparing and contrasting 4HPR's effects on premalignant PWR-1E and malignant DU-145 human prostate epithelial cells. 4HPR promoted a dose- and/or time-dependent apoptosis induction in PWR-1E and DU-145 cells, which was preceded by and dependent on an increase in mitochondrial ROS production. In this regard, the PWR-1E cells were more sensitive than the DU-145 cells, and they consumed roughly twice as much oxygen as the DU-145 cells suggesting oxidative phosphorylation was higher in the premalignant cells. Interestingly, increasing the $[Ca^{2+}]$ in the culture medium of the PWR-1E cells attenuated their proliferation as well as their mitochondrial bioenergetic capacity and 4HPR's cytotoxic effects. Correspondingly, the respiration-deficient derivatives (i.e., ρ^0 cells lacking mitochondrial DNA) of DU-145 cells were markedly resistant to 4HPR-induced ROS production and apoptosis. Together, these observations implied that the reduction of mitochondrial bioenergetics protected PWR-1E and DU-145 cells against the cytotoxic effects of 4HPR, and support the concept that oxidative phosphorylation is an essential determinant in 4HPR's apoptogenic signaling in transformed human prostate epithelial cells.

Keywords

4HPR; Apoptosis; Mitochondrial bioenergetics; Chemoprevention; Prostate cancer

Introduction

Prostate cancer is one of the most frequently diagnosed tumors, and the second leading cause of cancer death among men in the United States. Despite the routine use of diagnostic indicators

Numsen.Hail@UCDenver.edu .

The authors declare that they have no conflict of interest.

for prostate cancer development (e.g., prostate-specific antigen screening), a high cure rate for localized disease, and an increased understanding of prostate cancer biology, most men who develop metastatic prostate cancer will succumb to this disease. Thus, it is clear that effective prostate cancer prevention strategies would spare many men the burden of diagnosis and treatment [1,2].

Cancer chemoprevention uses natural or synthetic chemical agents to modulate carcinogenesis thereby lowering the risk of developing invasive or clinically significant disease. For example, an apoptogenic chemopreventive agent could intervene in the promotion phase of carcinogenesis to eliminate premalignant cells before they progress to malignancy [3]. Given the indolent nature of prostate tumorigenesis, chemoprevention would appear to be a potentially highly effective approach for deferring malignancy [4].

N-(4-Hydroxyphenyl)retinamide (4HPR, also known as fenretinide) has emerged as a promising cancer chemopreventive agent based on the cumulative results of numerous in vitro and animal studies, as well as chemoprevention clinical trials [5]. With respect to prostate cancer chemoprevention, dietary administration of 4HPR prevents prostate tumor growth [6, 7] and metastasis [6,8] in animals, and 4HPR functions as an apoptosis inducer in human prostate cancer cells in culture [9–11]. Many in vitro studies utilizing various premalignant and malignant cell types, including malignant human prostate epithelial cells, have shown that 4HPR's major apoptogenic features include the production of reactive oxygen species (ROS) and mitochondrial disruption (reviewed in [5]).

The metabolic function of human prostate peripheral zone glandular epithelial cells is unique. Compared to other epithelial cell types, normal prostate glandular epithelial cells sequester zinc, which inhibits the activity of mitochondrial aconitase, an enzyme involved in citrate metabolism through its participation in the Krebs cycle. This causes Krebs cycle truncation and the accumulation of high concentrations of citrate, which these cells normally secrete into the prostatic fluid. Truncation of the Krebs cycle by mitochondrial aconitase inactivation also inhibits oxidative phosphorylation (OXPHOS). Hence, normal prostate glandular epithelial cells typically exhibit suppressed mitochondrial bioenergetics, and the ROS production that accompanies it [2,12].

Conversely, the transformation of prostate epithelial cells is believed to be associated with an early metabolic switch that leads to a decrease in intracellular zinc accumulation, an increase in citrate oxidation by aconitase, and the subsequent production of reducing equivalents (e.g., NADH) that can be utilized by the mitochondrial electron transport chain to encourage OXPHOS [2,12]. Moreover, a recent human trial has reported decreased citrate levels in prostate tissue can serve as an important biomarker for prostate cancer development [13]. The stimulation of mitochondrial bioenergetics in transformed prostate epithelial cells implies a concomitant increase in oxygen consumption, ATP generation, and ROS production compared to their normal counterparts. These changes in the bioenergetic phenotype of transformed prostate epithelial cells may provide a proliferative advantage that is required to establish tumorigenesis. Likewise, the enhanced ROS production in transformed prostate epithelial cells resulting from heightened mitochondrial bioenergetics could act as a feed-forward mechanism for tumor promotion in the prostate [1,12,14,15]. These anomalous metabolic effects may not be specific to prostate cancer development. Indeed, a recent elegant study has shown that primary human fibroblasts serially transduced with oncogenes representing a progression of tumorigenic potential exhibited consecutive increases in ATP generation, oxygen consumption, and ROS production [16].

The possibility tumorigenesis in the prostate is driven to some extent by enhanced mitochondrial bioenergetics in transformed prostate epithelial cells is intriguing. These

bioenergetic/redox features could conceivably sensitize the transformed cells to apoptosis induction by a prooxidant/anti-mitochondrial cancer chemopreventive agent [17]. Couple these concepts with the possibility that 4HPR-induced ROS production is associated with mitochondrial bioenergetics and required for apoptosis induction in transformed prostate epithelial cells in vitro, and this would advocate a prospective mechanistic basis for 4HPR-mediated prostate cancer chemoprevention in vivo. This study, which is an extension of our previous studies of 4HPR's apoptogenic activity in human skin cancer cells [18,19], investigated this tenet by characterizing 4HPR-induced apoptosis in premalignant and malignant prostate epithelial cells. The information presented here illustrates that 4HPR can exploit, as a pharmacological target, mitochondrial bioenergetics in these cells to trigger ROS production, mitochondrial disruption, and apoptosis in vitro, which may be an important mechanism for suppressing prostate tumorigenesis in vivo.

Materials and methods

Cell culture and reagents

The PWR-1E and DU-145 human prostate epithelial cells and the synthetic androgen R1881 were kindly provided by Dr. Rajesh Agarwal (University of Colorado Denver School of Pharmacy, Aurora, CO). The PWR-1E cells were cultured in keratinocyte growth medium (KGM), consisting of keratinocyte basal medium supplemented with 100 ng/ml human recombinant epidermal growth factor, 0.4% bovine pituitary extract (Invitrogen Corporation, Carlsbad, CA), and 1 nM R1881 as described previously [20]. For certain experiments, the PWR-1E cells were cultured for 6 d in the medium described above that had the [Ca^{2+}] increased to 1.9 mM by adding $CaCl_2$.

The DU-145 cells and their respiration-deficient derivatives lacking mitochondrial DNA (mtDNA, i.e., ρ^0 clones) were cultured in Dulbecco's Modified Eagle's medium containing 4.5 g/l D-glucose and 110 μg/ml pyruvate (Invitrogen) supplemented with 50 μg/ml uridine (Sigma–Aldrich Chemical Co., St. Louis, MO), and 2% fetal bovine serum (Invitrogen). The ρ^0 derivatives of DU-145 cells were isolated using ethidium bromide (EthBr) as described previously [21]. All of the cell cultures were incubated at 37°C in humidified air containing 5% CO_2. Treatment with 4HPR and/or other agents was performed on sub-confluent (i.e., ~50% confluent) cultures.

4HPR was kindly provided by Dr. James A. Crowell (Division of Cancer Prevention, National Cancer Institute, Bethesda, MD). Dimethyl sulfoxide (Me_2SO), $CaCl_2$, 2′,7′-dichlorofluorescin diacetate, dihydroethidium, 3,3′-dihexyloxacarbocyanine iodide [$DiOC_6(3)$], EthBr (10 mg/ml solution), 2-heptyl-4-hydroxyquinoline-*N*-oxide (HQNO), KCN, and *N*-acetyl-L-cysteine (NAC) were purchased from Sigma–Aldrich. Hoechst 33342 (10 mg/ml solution) was purchased from Invitrogen.

Apoptosis assays and cell cycle analysis

Apoptotic DNA fragmentation was ascertained by cell staining using a hypotonic solution of propidium iodide (PI) [22]. The cell suspensions were analyzed by flow cytometry for PI fluorescence intensity. This procedure was also used to examine the cellular DNA content of viable cells relative to their cell cycle progression. The externalization of cell membrane phosphatidylserine was analyzed by the annexin V-based technique as described previously [22] using a kit purchased from BD Biosciences (San Jose, CA). Following treatment with 4HPR or Me_2SO, PWR-1E cells were harvested and stained with annexin V-conjugated fluorescein isothiocyanate (FITC) and PI according to the manufacture's instructions. The cell suspensions were then analyzed by flow cytometry for FITC and PI fluorescence intensity. Flow cytometry was performed with a Becton Dickinson FACScan flow cytometer (BD

Biosciences, San Jose, CA), and data analysis was accomplished using WinMDI version 2.8 software (copyright Dr. Joseph Trotter 1993–2000, Scripps Research Institute, La Jolla, CA).

Assay for mitochondrial inner transmembrane potential

The cationic dye $DiOC_6(3)$ was used to evaluate mitochondrial inner transmembrane potential ($\Delta\Psi_m$) [22]. The cells were treated in their culture medium for the indicated times. About 20 min before the cells were harvested, $DiOC_6(3)$ was added to the culture medium to give a final concentration of 40 nM. The cells were harvested and analyzed immediately for $DiOC_6(3)$ fluorescence intensity using flow cytometry. For the experiment comparing the retention of $DiOC_6(3)$ by DU-145 and DU-145 ρ^0 cells, the cells were harvested and counted. Approximately 2×10^6 cells were resuspended in 2 ml of Ca^{2+}-free phosphate-buffered saline (PBS) at 37°C, which contained 40 nM $DiOC_6(3)$. The cell suspensions were incubated at 37° C for 20 min and analyzed immediately for $DiOC_6(3)$ fluorescence intensity via flow cytometry.

Quantitative determination of ROS generation

The generation of intracellular ROS was measured using 2′,7′-dichlorofluorescin diacetate [19]. Cells were seeded in 6-well tissue culture plates and allowed to reach ~50% confluence. The wells were washed twice with 2 ml of Krebs–Ringer buffer (KRB, 10 mM D-glucose, 120 mM NaCl, 4.5 mM KCl, 0.15 mM $CaCl_2$, 0.7 mM Na_2HPO_4, 1.5 mM NaH_2PO_4, and 0.5 mM $MgCl_2$ [pH 7.4 at 37°C], Sigma–Aldrich) and covered with 2 ml of KRB containing 10 μg/ml 2′,7′-dichlorofluorescin diacetate and the indicated agent(s) or Me_2SO (control). Fluorescence emission at 538 nm (representing 2′,7′-dichlorofluorescein (DCF) production) was measured immediately following mixing (time zero) and subsequently at 30-min intervals over a 150-min period using a SpectraMax Gemini EM dual-scanning microplate spectrofluorimeter (Molecular Devices, Sunnyvale, CA).

Measurement of oxygen consumption in cultured cells

Oxygen consumption was measured polarographically using a Clark-type oxygen electrode and YSI Model 5300A Biological Oxygen Monitor (Yellow Spring Instrument Co., Yellow Springs, OH) [22]. Once harvested, the cells were counted, resuspended at a density of ~1×10^6 cells/ml in fresh medium at 37°C, and 3 ml of the cell suspension was placed in a 3-ml respiration chamber. Oxygen consumption was measured over a 10- to 15-min period. The oxygen consumption measurements were recorded and analyzed using Logger Pro version 3.2 software (Vernier Software and Technology, Beaverton, OR).

Epifluorescence microscopy

The medium was removed from the PWR-1E cell cultures following treatment, and the cultures were washed with 5 ml of KRB at 37°C. The cells were then incubated at 37°C for 20 min in 5 ml of KRB containing 40 nM $DiOC_6(3)$ and 5 μM dihydroethidium. This staining solution was replaced with 5 ml KRB at 37°C. For the experiments examining the retention of $DiOC_6(3)$ in untreated cells, the cultures were washed with 5 ml of KRB at 37°C. The cells were then incubated at 37°C for 20 min in 5 ml of KRB containing 40 nM $DiOC_6(3)$ and 5 μg/ml Hoechst 33342 (a nuclear counterstain). This staining solution was replaced with 5 ml of KRB at 37°C. The cells were photographed using a Nikon TE2000 microscope and digital color camera (Nikon Instruments, Melville, NY). The intensity of the 120 W Hg lamp was set at 25% of maximum, and the image exposure time was set for 0.5 s.

Assessment of cytosolic cytochrome *c*

Extra-mitochondrial cytochrome *c* was determined as described previously [23] with some modifications. Briefly, PWR-1E cells were treated for the indicated times with 4HPR or

Me_2SO. The cells were harvested, washed once with 1 ml of PBS, and gently votrexed for 30 s in 80 μl of ice cold cell permeabilization buffer [250 mM sucrose, 1 mM EDTA, 80 mM KCl, 0.05% digitonin, 25 mM Tris, pH 6.8, 1 mM dithiothreitol, 1 μg/ml leupeptin, 1 μg/ml pepstatin, 1 μg/ml aprotinin, 1 mM benzamidine, and 0.1 mM phenylmethylsulfonyl fluoride (all from Sigma–Aldrich)]. The cell suspensions were centrifuged at 12,000 × *g* at 4°C for 5 min in order to separate the soluble protein fraction from the permeabilized cells. The supernatant proteins (~50 μl) were subjected to electrophoresis in a SDS–Polyacrylamide slab gel and evaluated using immunoblot analysis.

Immunoblot analyses

Cellular proteins were characterized as described previously [24]. Samples containing ~50 μg of total cellular protein were separated via electrophoresis through a SDS–polyacrylamide slab gel followed by transfer to a nitro-cellulose membrane (Bio-Rad Laboratories, Hercules, CA). The membrane was probed with the indicated antibodies. BCL-X_L, cytochrome *c*, epidermal growth factor receptor, and *β*-actin were purchased from Santa Cruz Biotechnology (Santa Cruz, CA). Cytochrome *c* oxidase subunit 2 was purchased from Invitrogen, mitochondrial aconitase was purchased from Sigma–Aldrich, and Mn superoxide dismutase was purchased from Upstate Cell Signaling Solutions (Lake Placid, NY). A horseradish peroxidase-linked secondary antibody was used to detect the primary antibody with an enhanced chemiluminescence kit (Amersham Biosciences Corp., Piscataway, NJ). The immunoblots were subjected to densitometric analysis using ImageJ software (National Institutes of Health, Bethesda, MD). The immunoblot band intensity was normalized as a percent of the loading control *β*-actin.

Assessment of the mtDNA content in cultured cells

A PCR procedure was used to detect the mtDNA sequences in the cellular DNA samples from DU-145 cells. The PCR reaction was conducted in a thermal cycler (GeneAmp PCR System 9700, Applied Biosystems, Foster City, CA) using a primers set that was specific for the detection of total mtDNA as described previously [21].

Statistical analyses

The statistical significance between the means of two groups or more was determined using a two-sided, unpaired *t* test or a one-way ANOVA with Dunnett's post test, respectively, (GraphPad InStat version 3.0 software, GraphPad Software, Inc., San Diego, CA). All means ± SD for triplicate samples were calculated with Microsoft Excel 2003 SP2 software (Microsoft Corporation, Seattle, WA). In all statistical analyses, the results were considered significant for $P < 0.05$.

Results

4HPR encourages dose- and time-dependent apoptosis in PWR-1E and DU-145 cells

Previously, a few in vitro studies have demonstrated that short-term (i.e., 24–48 h) exposures to low micromolar (i.e., 1–5 μM) concentrations of 4HPR could promote apoptosis in malignant human prostate epithelial cells like DU-145, LNCaP, and PC-3 cells [9–11]. However, scant mechanistic data have emerged from the aforementioned studies that would suggest a pharmacological target for 4HPR in the malignant cells or how this agent could function as a potential apoptogenic prostate cancer chemopreventive agent. Furthermore, the mechanistic aspects associated with 4HPR-induced apoptosis in premalignant human prostate epithelial cells have not been characterized in vitro. Expectedly, the apoptotic eradication of premalignant prostate epithelial cells would be the primary objective for prostate cancer chemoprevention by 4HPR in vivo.

Premalignant cells represent an early stage of cancer development, which can serve as a pre-determinant for possible future malignancy. Cell immortalization or the ability to overcome senescence is an essential initial step in the multistep process of carcinogenesis [25]. The PWR-1E cells were derived from normal prostate epithelial cells that were immortalized using the adenovirus-12/simian virus-40 hybrid virus [25]. The PWR-1E cells express the differentiation markers androgen receptor [20,25], prostate-specific antigen [20,25], and cytokeratin 18 [25] that are characteristic of peripheral zone epithelial cells. Webber et al. [25] also suggested that PWR-1E cells with their deregulated proliferation and p53 tumor suppressor function can serve as an in vitro model for investigating the activity of potential prostate cancer chemopreventive agents. Therefore, we used the PWR-1E cells as an in vitro representative of premalignant prostate epithelial cells.

We exposed the PWR-1E cells to increasing micromolar concentrations of 4HPR for 24 h and examined these cells for apoptotic DNA fragmentation. As shown in Fig. 1a, increasing the concentration of 4HPR promoted a concomitant escalation in the percentage of hypoploid cells (i.e., cells exhibiting DNA content below 300 fluorescence units of PI, Fig. 1a inset) in the treatment populations relative to the Me_2SO-treated controls. The 2.5- and 5-μM concentrations of 4HPR were effective in triggering apoptosis in ~50% or more of the treatment population after 24 h. Even after a 48-h exposure to 1 μM 4HPR, DNA fragmentation was detected in ~60% of the treatment population compared to ~9% in the control (data not shown).

Light microscopy revealed progressive nuclear condensation, membrane budding, and cell shrinkage typical of apoptosis [26] in the PWR-1E cells exposed to 5 μM 4HPR (Fig. 1b). In addition to the aforementioned morphological changes, most of the cells developed pearly cytoplasmic vacuolizations that can be observed in the image taken 6 h after 4HPR treatment. The cell shrinkage described above appeared to parallel plasma membrane remodeling because the externalization of phosphatidylserine could be detected in ~70% of the 4HPR-treated cells after 12 h, and ~50% of this population remained impervious to PI signifying an early stage of cell death. This was markedly different from the control where ~12% of the cells were FITC positive and most of these cells were also PI positive (Fig. 1b insets).

The PWR-1E cells also exhibited a time-dependent increase in DNA fragmentation during a 24-h exposure to 5 mM 4HPR (Fig. 1c). These results were compared with the possible apoptogenic effects of 5 mM 4HPR on the malignant (i.e., isolated from a brain metastasis, [10]) DU-145 prostate epithelial cells. Interestingly, the kinetics of a robust (i.e., occurring in ~50% or more of the treatment population) induction of cellular DNA fragmentation was noticeably slower in the DU-145 cells compared to the PWR-1E cells (Fig. 1c). Exposure to 4HPR caused the prevalent induction of apoptotic morphology in the DU-145 cells and cytoplasmic vacuolizations could be detected in many of these cells as well, but this was not obvious until roughly 24 h following treatment (data not shown).

4HPR-induced apoptosis is associated with mitochondrial disruption in certain cell systems [19,27]. Cytoplasmic vacuolization has also been attributed to mitochondrial disruption in apoptotic cells [22]. During a 6-h exposure to 5 mM 4HPR, we used the decreased retention of the cationic dye $DiOC_6(3)$ as a surrogate indicator of the dissipation of $\Delta\Psi_m$ in PWR-1E cells. Figure 1d illustrates the time-dependent decay of the mean channel $DiOC_6(3)$ fluorescence intensity in the PWR-1E cells exposed to 4HPR. We also observed the time-dependent increase in cytosolic cytochrome *c* in these cells during a similar exposure to 4HPR (Fig. 1d inset), suggesting that 4HPR triggered the liberation of this protein from the mitochondrial intermembrane space.

The mitochondrial permeability transition has been attributed to 4HPR-induced mitochondrial disruption in cultured cells [19,28]. We used epifluorescence microscopy to examine some of

the familiar features associated with this process in PWR-1E cells treated with 5 mM 4HPR for 6 or 12 h. Using $DiOC_6(3)$ and dihydroethidium staining, we expected to observe a loss of $DiOC_6(3)$ fluorescence intensity (detected previously, Fig. 1d) and an increase in ethidium fluorescence intensity (caused by the oxidation of dihydroethidium) indicative of anomalous mitochondrial ROS generation in the cells exposed to 4HPR. As shown in the PWR-1E control cells in Fig. 1e, the $DiOC_6(3)$ fluorescence revealed a bright green, thread-like mitochondrial network that was spread uniformly within the cytoplasm. These cells also showed weak red nuclear ethidium fluorescence. Ethidium intercalates nuclear DNA and it is thus retained by a cell largely irrespective of the integrity of its plasma membrane.

Conversely, the $DiOC_6(3)$ green fluorescence in the PWR-1E cells treated with 4HPR for 6 h was noticeably diminished in most of the cells and seemingly altogether absent in many of the cells. Generally, the $DiOC_6(3)$ staining appeared weak, punctate, and mostly perinuclear. Many of the cells treated with 4HPR for 6 h also displayed strong perinuclear and nuclear red ethidium fluorescence that appeared to reveal nuclear condensation in some of these cells. After 12 h, all of the 4HPR-treated cells apparently lost their ability to retain $DiOC_6(3)$, and the ethidium fluorescence revealed marked nuclear condensation and fragmentation (Fig. 1e). These apoptotic nuclear changes detected by the ethidium staining are essentially the same nuclear changes revealed by Hoechst 33342 staining in the apoptotic PWR-1E cells following 4HPR treatment (data not shown). However, Hoechst 33342 and similar dyes like 4′, 6-diamidino-2-phenylindole (DAPI) that are commonly used to monitor nuclear changes in cultured cells do not also denote ROS or oxidative stress in the frankly apoptotic cells as indicated by the ethidium staining, which, as mentioned previously, is the fluorescent DNA-binding derivative of oxidized dihydroethidium.

4HPR functions as a prooxidant in PWR-1E and DU-145 cells

Mitochondrial disruption may be a cause or consequence of apoptosis, and it can be triggered by a variety of factors including ROS, Ca^{2+}, and various chemical agents [29]. Since the mitochondrial changes detected in the PWR-1E cells exposed to 4HPR occurred well before marked cell shrinkage and DNA fragmentation, this strongly supported the idea that mitochondrial disruption was a cause, not a result, of cell death. There were no obvious changes in the retention of $DiOC_6(3)$ or the cellular redistribution of cytochrome *c* during the first 2 h of exposure to 4HPR in PWR-1E cells (Fig. 1d). This prompted the examination of ROS production in these cells to determine if 4HPR could trigger oxidative stress prior to mitochondrial disruption, which could serve as a possible prerequisite for apoptosis.

PWR-1E cells were treated with 1, 2.5, or 5 μM 4HPR and examined for ROS production using the oxidation of 2′,7′-dichlorofluorescin to DCF. During a 2.5-h exposure to 4HPR, we observed a dose- and time-dependent increase in DCF fluorescence intensity suggestive of enhanced ROS production in the PWR-1E cells. This increase could be detected as soon as 30 min following exposure to 4HPR (Fig. 2a). We repeated this assay using the DU-145 cells treated with 5 μM 4HPR. The increase in DCF fluorescence intensity caused by 4HPR appeared to follow similar kinetics observed in the PWR-1E cells. However, the time-dependent increase in DCF fluorescence intensity triggered by 5 μM 4HPR in the DU-145 cells was less than half that exhibited by the same concentration of 4HPR in roughly the same number of PWR-1E cells. The time-dependent increase in the DCF fluorescence intensity of the Me_2SO-treated control DU-145 cells was also only ~50% of that displayed by the same treatment in the PWR-1E cells (Fig. 2a).

Center *i* inhibitors of complex III of the mitochondrial electron transport chain conspicuously increased ROS generation by 4HPR in skin [18] and cervical [30] cancer cells, indicating the activity of dehydrogenases in complex I may contribute to redox cycling and ROS production by 4HPR [18]. The effect of the center *i* inhibitor HQNO [18] was examined on ROS production

by 4HPR in the DU-145 cells. Co-treating these cells with an equal molar concentration of HQNO caused a marked increase in the DCF fluorescence intensity compared to the increase in DCF fluorescence intensity triggered by 4HPR or HQNO alone (Fig. 2a). At ~19.7 fluorescence units/min, the rate of DCF fluorescence increase triggered by this combination was far more than additive of the rates of 4HPR (i.e., ~6.3 fluorescence units/min) plus HQNO (i.e., ~2.8 fluorescence units/min), and over 3 fold higher than 4HPR alone (Fig. 2a). Exposure to HQNO and 4HPR in the PWR-1E cells produced a 2.7 fold increase in the DCF fluorescence units/min compared to 4HPR alone (data not shown).

Since the DU-145 cells had a delayed apoptotic response to 5 μM 4HPR compared to the PWR-1E cells (Fig. 1c), we examined the expression of several redox-sensitive proteins in the DU-145 cells to potentially identify how ROS and/or oxidative stress was affecting these cells. Antiapoptotic BCL-2 family members like BCL-X_L are typically down regulated in cells during conditions of oxidative stress [26], and a previous study has shown the 4HPR-induced loss of BCL-X_L expression in DU-145 cells [10]. Cytochrome *c* oxidase (i.e., complex IV) subunit II that is encoded by mtDNA [31] and mitochondrial aconitase [32] are particularly sensitive to ROS damage, and the expression of epidermal growth factor receptor can be down regulated by ROS [33]. Furthermore, Mn superoxide dismutase can be up regulated in response to anomalous mitochondrial ROS production [32]. As shown in Fig. 2b, a 24-h exposure to 4HPR caused decreases of ~50% in the levels of mitochondrial aconitase, BCL-X_L, cytochrome *c* oxidase subunit II, and epidermal growth factor receptor. 4HPR treatment also caused a 40% increase in the level of Mn superoxide dismutase in the DU-145 cells.

In addition to enhanced ROS production, another common property of 4HPR-induced apoptosis is its inhibition by antioxidants (e.g., NAC and vitamin C) suggesting an essential role for ROS and oxidative stress in 4HPR's cytotoxicity [5]. If the initial ROS production triggered by 4HPR was consequential to cell death in the PWR-1E and DU-145 cells, suppressing this effect should diminish cell death. Indeed, pretreating these cells for 2 h with the antioxidant NAC [22] appreciably suppressed the rate of ROS generation by 5 μM 4HPR (Fig. 2c). NAC also markedly inhibited the DNA fragmentation following a 24-h exposure to 5 μM 4HPR in the PWR-1E cells or a 48-h exposure to the same concentration of 4HPR in the DU-145 cells (Fig. 2d).

Increasing the [Ca^{2+}] in the KGM of PWR-1E cells inhibits their proliferation, mitochondrial bioenergetics, and the cytotoxic effects of 4HPR

The culture conditions for the PWR-1E cells and DU-145 cells are very distinct, which may have contributed to the sensitivity of the PWR-1E cells to 4HPR-induced ROS and apoptosis. We investigated culturing the PWR-1E cells in the same medium as the DU-145 cells to determine if this would affect their sensitivity to 4HPR's cytotoxicity. However, changing the culture medium caused ~35% of the PWR-1E cells to undergo spontaneous apoptosis within the first 2 day (data not shown). The PWR-1E cells are reportedly sensitive to Ca^{2+} [25]. The KGM [Ca^{2+}] is ~75 μM, and the [Ca^{2+}] in the Dulbecco's Modified Eagle's medium with 2% fetal bovine serum is roughly 1.9 mM [34], suggesting that perhaps the increased medium [Ca^{2+}] triggered the initial cell loss in the PWR-1E cells. The KGM also did not contain serum. Consequently, it was possible the serum added to the Dulbecco's Modified Eagle's medium contained transforming growth factor-β, which has also been shown to suppress proliferation in PWR-1E cells [25].

We augmented the [Ca^{2+}] in the KGM to determine if we could mimic the effects we observed for the PWR-1E cells cultured in the Dulbecco's Modified Eagle's medium. Indeed, increasing the [Ca^{2+}] of the KGM to 1.9 mM caused cell death in ~30–40% of the PWR-1E cells during the first 2 day of culture (data not shown). However, after changing this medium every other day over 6 days the initial cells loss was followed by a modulation of proliferation and distinct

morphological and biochemical changes in the surviving PWR-1E cells. Compared to the parental cells, the cells cultured in high Ca^{2+} KGM underwent cell flattening, the loss of pleomorphism, increased cell-to-cell contact, a decrease in their nuclear to cytoplasmic ratio, and a loss of their mitochondrial network as evidenced by their weak stippled $DiOC_6(3)$ staining (Fig. 3a). After 6 days, almost all of the cells in the high Ca^{2+} KGM were in the G_0/G_1 phase (i.e., cells exhibiting DNA content around 400 fluorescence units of PI) of the cell cycle compared to the cells grown in KGM (Fig. 3b), suggesting that the high Ca^{2+} KGM caused growth suppression in the PWR-1E cells. Similar changes in proliferation and morphology have also been observed in normal prostate epithelial cells [34,35] and normal cutaneous keratinocytes [36] cultured in KGM containing a high (i.e., ≥660 μM) [Ca^{2+}].

The PWR-1E cells cultured in the high Ca^{2+} KGM also consumed markedly less O_2 compared to the parental PWR-1E cells (Fig. 3c), which seemingly provided a biochemical basis for the loss of $DiOC_6(3)$ retention by these cells. Normally, the O_2 consumption by the PWR-1E cells could be blocked using 1 mM of the complex IV inhibitor cyanide [21], suggesting that O_2 consumption in these cells resulted from mitochondrial bioenergetics (data not shown). It should also be noted that the PWR-1E cells were very difficult to trypsinize once they were cultured in the KGM containing 1.9 mM Ca^{2+}, and they could not be passed under these conditions inasmuch as the cells were unable to reattach to a tissue culture plate and presumably died via anoikis (data not shown).

Culturing the PWR-1E cells in the in high Ca^{2+} KGM diminished their growth and mitochondrial function. Therefore, we wanted to determine if these Ca^{2+}-induced effects would suppress the prooxidant and apoptogenic qualities of 4HPR. As shown in Fig. 4a, there was roughly a 2 fold increase in the 4HPR-induced ROS generation rate in the cells cultured in the high Ca^{2+} KGM compared to the ~8 fold increase in the ROS generation rate triggered by the same treatment in the PWR-1E cells cultured under normal conditions. The cells cultured in the high Ca^{2+} KGM also demonstrated resistance to 4HPR-induced apoptosis. There was visual evidence of some cell death in the form of floating cells (not shown), condensed cells, and cell fragments that were adherent to the cultures exposed to 4HPR for 24 h (Fig. 4b), which remained essentially unchanged after 48 h (data not shown). However, this was far less extensive compared to the fate of the 4HPR-treated PWR-1E cells cultured under their normal conditions (Fig. 1b). A 24-h exposure to 5 μM 4HPR also did not promote cytoplasmic vacuolizations in the viable PWR-1E cells cultured in the high Ca^{2+} KGM (Fig. 4b). Furthermore, the DNA fragmentation triggered in these cells after a 24-h exposure to 5 μM 4HPR was less than a third of that detected in the same cells cultured under their normal conditions (Fig. 4c).

The ρ^0 derivatives of DU-145 cells are markedly resistant to the cytotoxic effects of 4HPR

Ca^{2+} is commonly recognized as a growth inhibitory and differentiation-inducing agent in many epithelial cell types [34,36]. The effects of Ca^{2+} on the PWR-1E cells attest to its growth inhibitory potential in these cells. However, the same could not be said for the DU-145 cells, which were routinely propagated in medium containing a [Ca^{2+}] that was representative of a physiological Ca^{2+} level [34]. In our hands, the doubling time for the DU-145 cells was ~28 h. This rate was more rapid compared to ~33 h for the PWR-1E cells cultured in KGM with its sub-physiological [Ca^{2+}]. Given the myriad of possible reasons why Ca^{2+} affected the PWR-1E cells in the way that it did and the fact we were unable to culture of these cells in the high Ca^{2+} KGM long term, it could reasonably be argued that the acquired resistance to 4HPR-induced ROS and apoptosis in these cells was probably non-specific and perhaps related to the suppression of cell proliferation, since others have shown growth inhibition in hepatoma cells could repress 4HPR-induced apoptosis [37]. If the mitochondrial bioenergetic component of the Ca^{2+}-mediated effects reported for the PWR-1E cells was pivotal for their resistance to

4HPR-induced ROS and apoptosis, we should be able to recapitulate this effect in the DU-145 cells if we specifically knocked out their OXPHOS and maintained their normal culture conditions, which already included a physiological [Ca^{2+}].

The chronic treatment (i.e., ~8 weeks) of cultured cells with very low (e.g., 100 ng/ml) concentrations of EthBr is an established method for depleting mtDNA and inhibiting OXPHOS [22]. We probed for mtDNA sequences in the total cellular DNA derived from the parental DU-145 cells, and DU-145 cells exposed for 6 days or 8 weeks to 100 ng/ml EthBr. Exposing the DU-145 cells to EthBr for as little as 6 day reduced their mtDNA content by ~50%, and mtDNA sequences were not detected in four of the clones isolated after 8 weeks of EthBr exposure (Fig. 5a). Thus, we designated these cells as ρ^0 clones.

Upon examining the protein expression in the parental DU-145 cells and the ρ^0 clone 13 (Fig. 5b), we observed that mitochondrial aconitase expression was ~64% lower and, as expected, the mtDNA-encoded cytochrome *c* oxidase subunit II was absent in the ρ^0 cells. The expression of the apoptosis regulator BCL-X_L was unchanged, as was the expression of the growth regulator epidermal growth factor receptor. It should be noted that the ρ^0 clones proliferated slower than the parental DU-145 cells. The doubling time for the DU-145 ρ^0 clone 13 cells was ~47 h indicating mitochondrial bioenergetics contributed to the rate of cell proliferation in the parental DU-145 cells. There was also a slight (i.e., ~27%) reduction in the expression of Mn superoxide dismutase in the ρ^0 cells. Besides the expression of cytochrome *c* oxidase subunit II, perhaps the expression of mitochondrial aconitase and Mn superoxide dismutase were intimately linked to the bioenergetic phenotype of the parental DU-145 cells.

Interestingly, the O_2 consumption by the PWR-1E cells under their normal culture conditions (Fig. 3c) was almost twice that exhibited by the parental DU-145 cells (Fig. 5c). We also observed decreases in the O_2 consumption by the DU-145 cells exposed for varying times to EthBr, which linked this process to the cellular mtDNA content. As observed for the PWR-1E cells (data not shown), the O_2 consumption by the parental DU-145 cells and the DU-145 cells exposed to EthBr for 6 days was sensitive to cyanide signifying a mitochondrial origin. The O_2 consumption in the DU-145 ρ^0 clone 13 cells was apparently cyanide-insensitive and ~16% of the O_2 consumption observed in the parental cells. Together, these observations affirmed the ρ^0 cells were functionally deficient in mitochondrial bioenergetics.

Morphologically, the ρ^0 clones were slightly larger than the parental DU-145 cells, and they exhibited a granular cytoplasm. These cells also had a disorganized mitochondrial network compared to the parental cells as illustrated by their punctate $DiOC_6(3)$ staining (Fig. 5d). A quantitative evaluation of the $DiOC_6(3)$ staining using flow cytometry revealed the fluorescence intensity of the ρ^0 cells was ~30% of that measured in the parental cells (Fig. 5d inset).

When the parental and ρ^0 clone 13 DU-145 cells were exposed to 5 μM 4HPR, we observed less than a 2 fold increase in the rate of 4HPR-induced ROS generation in the ρ^0 cells compared to the ~6.5-fold increase triggered by the same treatment in the parental cells (Fig. 6a). Correspondingly, and in stark contrast to the parental cells, a 48-h exposure to 5 μM 4HPR caused no visual manifestations of cytotoxicity in the DU-145 ρ^0 clone 13 cells (Fig. 6b). Moreover, the DNA fragmentation in the four DU-145 ρ^0 clones treated with 5 μM 4HPR for 48 h was neither biologically or statistically significant compared to that observed in the Me_2SO-treated controls (Fig. 6c).

Discussion

Extensive success in prostate cancer chemoprevention has been largely unachieved. For example, the selenium and vitamin E cancer prevention trial (SELECT) was the largest and

most ambitious prostate cancer prevention trial to date. Unfortunately, the initial independent review of the SELECT data carried out in September and October of 2008 revealed that selenomethionine and vitamin E supplements, taken either alone or together for an average of 5 years, were ineffective in preventing prostate cancer development, which prompted the early termination of SELECT by the National Cancer Institute. Thus, in order to continue the mission of prostate cancer chemoprevention that was the strategic initiative behind SELECT, we must expeditiously identify and characterize novel chemical agents that are potentially effective in this regard.

Since 4HPR has consistent apoptotic effects in vitro, this property is generally believed to constitute a basis for the anticancer activity of this compound in vivo [5]. Low micromolar (i.e., 1–10 μM) concentrations of 4HPR that routinely trigger apoptosis in transformed cells in vitro [5] can be attained in human plasma. For example, children with neuroblastoma have received oral doses of 4HPR as high as 4,000 mg/m^2/d for 4 weeks with no dose-limiting toxicity. This dose resulted in roughly a 13 μM sustained plasma concentration of 4HPR [38]. Furthermore, novel formulations of 4HPR like the recently described organized lipid matrix, LYM-X-SORB, are promising to deliver even higher levels of 4HPR to plasma and presumably target tissues within the body [39]. These observations and the results presented in this study indicate that 4HPR could facilitate an apoptogenic prostate cancer chemopreventive effect in humans.

Short-term exposures to 4HPR cause anomalous ROS production in various types of transformed cells in vitro. This ROS production has been designated as the causal factor for triggering a panoply of aberrant cellular events including enhanced ceramide production, diminished mitochondrial bioenergetics, the induction of the mitochondrial permeability transition, the up-regulation of death receptors, endoplasmic reticulum stress, lysosomal disruption, increased stress kinase signal transduction, the induction of proapoptotic BCL-2 family members and the suppression of antiapoptotic BCL-2 family members, and the initiation of the DNA damage response, to name a few, which presumably regulated cell death in these transformed cells [5]. There are numerous effectors of apoptosis, all of which ultimately contribute to the degradation and demise of the target cell [26]. However, since the common element associated with 4HPR-induced apoptosis appears to be its initiation by anomalous ROS production, it seems logical to focus on this feature of apoptosis rather than the effectors of this process. After all, the characterization of the initiation event of 4HPR-induced apoptosis in transformed cells will provide an upstream cellular/molecular pharmacological target that is ultimately responsible for the putative anticancer effect.

There is limited information described in the literature distinct from the use of antioxidants like NAC to block 4HPR-induced ROS production and apoptosis (Fig. 2c, d) that points to a biochemical/cell physiological underpinning for the regulation of 4HPR's prooxidant effects in transformed cells in vitro. This evidence and the cell physiological/phenotypic (e.g., the enhanced mitochondrial bioenergetics associated with prostate tumorigenesis discussed previously in the Introduction) characteristics of transformed cells in vivo, could provide a possible mechanistic basis for this agent's anticancer effect. In skin [18] and cervical [30] carcinoma cells, and the premalignant and malignant prostate epithelial cells described in this work, 4HPR appears to redox cycle within the mitochondrial electron transport chain. Specifically, in this study co-treatment of the PWR-1E and DU-145 cells with 4HPR and the complex III inhibitor HQNO greatly enhanced the DCF fluorescence compared to that exhibited by 4HPR alone (please see the Results text and Fig. 2a). These results suggested that 4HPR was redox cycling in these cells at the level of the mitochondrial electron transport chain. Furthermore, the decreased expression of mitochondrial aconitase and cytochrome *c* oxidase subunit II and the enhanced Mn superoxide dismutase expression in the DU-145 cells following exposure to 4HPR (Fig. 2b) implied these cells encountered enhanced mitochondrial ROS

production and/or oxidative stress. Finally, when the oxygen consumption, as an indicator of OXPHOS, was decreased in either the PWR-1E cells by a high [Ca^{2+}] in their tissue culture medium (Fig. 3) or the DU-145 cells by the depletion of mtDNA in these cells (Fig. 5) the prooxidant and apoptogenic effects of 4HPR were greatly diminished or altogether lost.

The prominent site of 4HPR-induced ROS may differ depending on cell type. Interestingly, a recent study examining the apoptogenic features of 4HPR in human head and neck squamous cell carcinoma cells has shown the suppression of the plasma membrane NADPH oxidase complex inhibited 4HPR-indiced ROS and apoptosis. Thus, the authors of this study suggested this redox enzyme complex was the primary site of 4HPR-induced ROS in these cells [40]. Compared to their parental counterparts, we have shown substantially attenuated, but not completely inhibited, 4HPR-induced ROS production in the DU-145 ρ^0 cells examined in this study (Fig. 6a), and also in ρ^0 human skin cancer cells characterized previously [18]. Therefore, we must assume there was a site or sites other than the mitochondrial electron transport chain where 4HPR could possibly undergo redox cycling reactions. However, the residual ROS triggered by 4HPR in the ρ^0 cells was evidently inadequate to cause cytotoxicity in these cells (e.g., Fig. 6b, c, and [18]). Likewise, the PWR-1E cells cultured in the high Ca^{2+} KGM also exhibited a loss of their mitochondrial bioenergetic capacity (Fig. 3c), but still had a residual 4HPR-induced ROS production (Fig. 4a). However, as with the ρ^0 DU-145 cells, their sensitivity to apoptosis induction by 4HPR was also greatly diminished (Fig. 4b, c). Furthermore, the loss of 4HPR-induced ROS in the ρ^0 DU-145 cells was probably not due to the activity of an antioxidant enzyme, at least not that of Mn superoxide dismutase, which was actually expressed at a lower level in the respiration deficient cells compared to their parental counterparts (Fig. 5b). While it is possible the plasma membrane NADPH oxidase complex contributed to ROS production by 4HPR in the premalignant and malignant prostate epithelial cells evaluated in this study, our results strongly suggest that mitochondrial bioenergetics was the predominant regulator for this process, and this ROS production was a necessary and sufficient condition to promote cell death.

In this study we observed obvious differences in the O_2 consumption (Figs. 3c, 5c) and the constitutive ROS generation (Fig. 2a) in the PWR-1E and DU-145 cells signifying that the bioenergetic phenotypes of these cells were dissimilar and seemingly more oxidative in our premalignant representative PWR-1E cells. Our ability to isolate an entirely glycolytic bioenergetic phenotype (i.e., the ρ^0 cells, Fig. 5) of the DU-145 cells implied that the malignant cells could sustain their viability and proliferative capacity by exhibiting plasticity in their energy generating strategy, which is a hallmark of malignancy [16].

As we alluded to in the Introduction, the protracted promotion stage of prostate carcinogenesis may afford a window of opportunity where 4HPR could be useful in suppressing malignancy. For example, it has been estimated that <1% of the normal epithelial cells in the adult human prostate undergo routine cell division [41]. However, the aberrant proliferation of transformed prostate epithelial cells, perhaps resulting from enhanced mitochondrial bioenergetics, ROS, and nurturing microenvironmental factors like angiogenesis and the appropriate tissue O_2 tension, could potentially lead to the establishment of a premalignant lesion and the disruption of prostate tissue homeostasis (Fig. 7). The observations of 4HPR-induced ROS and apoptosis in the PWR-1E cells (Figs. 1 and 2), along with the bioenergetic and proliferative characteristics of these cells under their normal low Ca^{2+} culture conditions (Fig. 3), suggested that 4HPR was effective in triggering mitochondrial ROS and mitochondrial disruption in these cells, which may be an important mechanism for preventing prostate malignancy. Furthermore, if in vivo microenvironmental factors like hypoxia do not enforce a predominately glycolytic bioenergetic phenotype (e.g., one that is characteristic of the Warburg effect) in malignant prostate epithelial cells (e.g., DU-145, Figs. 5 and 7) 4HPR may also have the ability to trigger ROS and apoptosis to eradicate these cells (Figs. 1,2). Hypoxia appears to be an important

environmental regulator of 4HPR-induced ROS and apoptosis in vitro [5]. We envision that the mechanistic evidence regarding the prooxidant and apoptogenic effects of 4HPR in transformed human prostate epithelial cells provided by this study would warrant continued investigations of 4HPR in the prevention of prostate cancer.

Acknowledgments

This work was supported by the National Institutes of Health (Grant CA133901-01 to Numsen Hail, Jr.) and the University of Colorado Denver School of Pharmacy.

Abbreviations

4HPR	*N*-(4-Hydroxyphenyl)retinamide
DCF	2′,7′-Dichlorofluorescein
$\Delta\Psi_m$	Mitochondrial inner transmembrane potential
$DiOC_6(3)$	3,3′-Dihexyloxacarbocyanine iodide
EthBr	Ethidium bromide
FITC	Fluorescein isothiocyanate
HQNO	2-Heptyl-4-hydroxyquinoline-*N*-oxide
KGM	Keratinocyte growth medium
Me_2SO	Dimethyl sulfoxide
mtDNA	Mitochondrial DNA
NAC	*N*-Acetyl-L-cysteine
OXPHOS	Oxidative phosphorylation
PI	Propidium iodide
ρ^0	Respiration-deficient cells lacking mtDNA
ROS	Reactive oxygen species
SELECT	Selenium and vitamin E cancer prevention trial

References

1. Chen JZ, Kadlubar FF. Mitochondrial mutagenesis and oxidative stress in human prostate cancer. J Environ Sci Health C Environ Carcinog Ecotoxicol Rev 2004;22:1–12. [PubMed: 15845219]
2. Costello LC, Franklin RB, Feng P. Mitochondrial function, zinc, and intermediary metabolism relationships in normal prostate and prostate cancer. Mitochondrion 2005;5:143–153. doi:10.1016/j.mito.2005.02.001. [PubMed: 16050980]
3. Sun SY, Hail N Jr, Lotan R. Apoptosis as a novel target for cancer chemoprevention. J Natl Cancer Inst 2004;96:662–672. [PubMed: 15126603]
4. Bettuzzi S, Brausi M, Rizzi F, Castagnetti G, Peracchia G, Corti A. Chemoprevention of human prostate cancer by oral administration of green tea catechins in volunteers with high-grade prostate intraepithelial neoplasia: a preliminary report from a one-year proof-of-principle study. Cancer Res 2006;66:1234–1240. doi:10.1158/0008-5472.CAN-05-1145. [PubMed: 16424063]
5. Hail N Jr, Kim HJ, Lotan R. Mechanisms of fenretinide-induced apoptosis. Apoptosis 2006;11:1677–1694. doi:10.1007/s10495-006-9289-3. [PubMed: 16850162]
6. Pollard M, Luckart PH, Sporn MB. Prevention of primary prostate cancer by N-4-hydroxyphenyl retinamide. Cancer Res 1991;51:3610–3611. [PubMed: 1829024]

7. Pienta KJ, Nguyen NM, Lehr JE. Treatment of prostate cancer in the rat with the synthetic retinoid fenretinide. Cancer Res 1993;53:224–226. [PubMed: 7678070]
8. Shaker MR, Yang G, Timme TL, et al. Dietary 4-HPR suppresses the development of bone metastasis in vivo in a mouse model of prostate cancer progression. Clin Exp Metastasis 2000;18:429–438. doi: 10.1023/A:1010905309570. [PubMed: 11467776]
9. Hursting SD, Shen JC, Sun XY, Wang TT, Phang JM, Perkins SN. Modulation of cyclophilin gene expression by *N*-4-(hydroxyphenyl)retinamide: association with reactive oxygen species generation and apoptosis. Mol Carcinog 2002;33:16–24. doi:10.1002/mc.10020. [PubMed: 11807954]
10. Sun S-Y, Yue P, Lotan R. Induction of apoptosis by *N*-(4-hydroxyphenyl)retinamide and its association with reactive oxygen species, nuclear retinoic acid receptors, and apoptosis related genes in human prostate carcinoma cells. Mol Pharmacol 1999;55:403–410. [PubMed: 10051523]
11. Hsieh TC, Wu JM. Effects of fenretinide (4-HPR) on prostate LNCaP cell growth, apoptosis, and prostate-specific gene expression. Prostate 1997;33:97–104. doi:10.1002/(SICI)1097-0045 (19971001)33:2<97::AID-PROS3>3.0.CO;2-J. [PubMed: 9316650]
12. Dakubo GD, Parr RL, Costello LC, Franklin RB, Thayer RE. Altered metabolism and mitochondrial genome in prostate cancer. J Clin Pathol 2006;59:10–16. doi:10.1136/jcp.2005.027664. [PubMed: 16394275]
13. Serkova NJ, Gamito EJ, Jones RH, et al. The metabolites citrate, myo-inositol, and spermine are potential age-independent markers of prostate cancer in human expressed prostatic secretions. Prostate 2008;68:620–628. doi:10.1002/pros.20727. [PubMed: 18213632]
14. Petros JA, Baumann AK, Ruiz-Pesini E, et al. mtDNA mutations increase tumorigenicity in prostate cancer. Proc Natl Acad Sci USA 2005;102:719–724. doi:10.1073/pnas.0408894102. [PubMed: 15647368]
15. Venkataraman S, Jiang X, Weydert C, et al. Manganese superoxide dismutase overexpression inhibits the growth of androgen-independent prostate cancer cells. doi:10.1038/sj.onc.1208145. Oncogene 2005;24:77–89. [PubMed: 15543233]
16. Ramanathan A, Wang C, Schreiber SL. Perturbational profiling of a cell-line model of tumorigenesis by using metabolic measurements. Proc Natl Acad Sci USA 2005;26:5992–5997. doi: 10.1073/pnas. 0502267102. [PubMed: 15840712]
17. Hail N Jr, Cortes M, Drake EN, Spallholz JE. Cancer chemoprevention: a radical perspective. Free Radic Biol Med 2008;45:97–110. doi:10.1016/j.freeradbiomed.2008.04.004. [PubMed: 18454943]
18. Hail N Jr, Lotan R. Mitochondrial respiration is uniquely associated with the prooxidant and apoptotic effects of *N*-(4-hydroxyphenyl)retinamide. J Biol Chem 2001;276:45614–45621. doi: 10.1074/ jbc.M106559200. [PubMed: 11546781]
19. Hail N Jr, Lotan R. Mitochondrial permeability transition is a central coordinating event in *N*-(4-hydroxyphenyl)retinamide-induced apoptosis. Cancer Epidemiol Biomarkers Prev 2000;9:1293–1301. [PubMed: 11142414]
20. Deep G, Oberlies NH, Kroll DJ, Agarwal R. Isosilybin B causes androgen receptor degradation in human prostate carcinoma cells via PI3 K-Akt-Mdm2-mediated pathway. Oncogene 2008;27:3986–3998. doi:10.1038/onc.2008.45. [PubMed: 18332867]
21. Hail N Jr, Youssef EM, Lotan R. Evidence supporting a role for mitochondrial respiration in apoptosis induction by the synthetic retinoid CD437. Cancer Res 2001;61:6698–6702. [PubMed: 11559538]
22. Hail N Jr. Mitochondrial reactive oxygen species affect sensitivity to curcumin-induced apoptosis. Free Radic Biol Med 2008;44:1382–1393. doi:10.1016/j.freeradbiomed.2007.12.034. [PubMed: 18206126]
23. Pique M, Barragan M, Dalmau M, Bellosillo B, Pons G, Gil J. Aspirin induces apoptosis through mitochondrial cytochrome *c* release. FEBS Lett 2000;480:193–196. doi:10.1016/S0014-5793(00) 01922-0. [PubMed: 11034327]
24. Zeng Z, Samudio IJ, Zhang W, et al. Simultaneous inhibition of PDK1/AKT and Fms-like tyrosine kinase 3 signaling by a small-molecule KP372–1 induces mitochondrial dysfunction and apoptosis in acute myelogenous leukemia. Cancer Res 2006;66:3737–3746. doi: 10.1158/0008-5472.CAN-05-1278. [PubMed: 16585200]
25. Webber MM, Bello D, Kleinman HK, Wartinger DD, Williams DE, Rhim JS. Prostate specific antigen and androgen receptor induction and characterization of an immortalized adult human prostatic

epithelial cell line. Carcinogenesis 1996;17:1641–1646. doi:10.1093/carcin/17.8.1641. [PubMed: 8761420]

26. Hail N Jr, Carter BZ, Konopleva M, Andreeff M. Apoptosis effectors mechanisms: a requiem performed in different keys. Apoptosis 2006;11:889–904. doi:10.1007/s10495-006-6712-8. [PubMed: 16547589]
27. Boya P, Morales MC, Gonzalez-Polo RA, et al. The chemopreventive agent *N*-(4-hydroxyphenyl) retinamide induces apoptosis through a mitochondrial pathway regulated by proteins from the Bcl-2 family. Oncogene 2003;22:6220–6230. doi:10.1038/sj.onc.1206827. [PubMed: 13679861]
28. Cuello M, Coats AO, Darko I, et al. *N*-(4-hydroxyphenyl) retinamide (4HPR) enhances TRAIL-mediated apoptosis through enhancement of a mitochondrial-dependent amplification loop in ovarian cancer cell lines. Cell Death Differ 2004;11:527–541. doi:10.1038/sj.cdd.4401387. [PubMed: 14765134]
29. Hail N Jr. Mitochondria: a novel target for the chemoprevention of cancer. Apoptosis 2005;10:687–705. doi:10.1007/s10495-005-0792-8. [PubMed: 16133861]
30. Suzuki S, Higuchi M, Proske RJ, Oridate N, Hong WK, Lotan R. Implication of mitochondria-derived reactive oxygen species, cytochrome *c* and caspase-3 in *N*-(4-hydroxyphenyl)retinamide-induced apoptosis in cervical carcinoma cells. Oncogene 1999;18:6380–6387. doi:10.1038/sj.onc.1203024. [PubMed: 10597238]
31. Lee HC, Wei YH. Mitochondrial biogenesis and mitochondrial DNA maintenance of mammalian cells under oxidative stress. Int J Biochem Cell Biol 2005;37:822–834. doi:10.1016/j.biocel.2004.09.010. [PubMed: 15694841]
32. Turrens JF. Mitochondrial formation of reactive species. J Physiol 2003;522:335–344. doi:10.1113/jphysiol.2003.049478. [PubMed: 14561818]
33. Zhuang S, Ouedraogo GD, Kochevar IE. Downregulation of epidermal growth factor receptor signaling by singlet oxygen through activation of caspase-3 and protein phosphatases. Oncogene 2003;22:4413–4424. doi:10.1038/sj.onc.1206604. [PubMed: 12853978]
34. Dalrymple S, Antony L, Xu Y, et al. Role of notch-1 and E-cadherin in the differential response to calcium in culturing normal versus malignant prostate cells. Cancer Res 2005;65:9269–9279. doi:10.1158/0008-5472.CAN-04-3989. [PubMed: 16230388]
35. Chaproniere DM, McKeehan WL. Serial culture of single adult human prostatic epithelial cells in serum-free medium containing low calcium and a new growth factor from bovine brain. Cancer Res 1986;46:819–824. [PubMed: 3000587]
36. Tamiji S, Beauvillain JC, Mortier L, et al. Induction of apoptosis-like mitochondrial impairment triggers antioxidant and Bcl-2-dependent keratinocyte differentiation. J Invest Dermatol 2005;125:647–658. doi:10.1111/j.0022-202X.2005.23885.x. [PubMed: 16185262]
37. You KR, Wen J, Lee ST, Kim DG. Cytochrome *c* oxidase subunit III: a molecular marker for *N*-(4-hydroxyphenyl)retina-mide-induced oxidative stress in hepatoma cells. J Biol Chem 2002;277:3870–3877. doi:10.1074/jbc.M109284200. [PubMed: 11698412]
38. Garaventa A, Luksch R, Lo Piccolo MS, et al. Phase I trial and pharmacokinetics of fenretinide in children with neuroblastoma. Clin Cancer Res 2003;9:2032–2039. [PubMed: 12796365]
39. Maurer BJ, Kalous O, Yesair DW, et al. Improved oral delivery of N-(4-hydroxyphenyl)retinamide with a novel LYMX-SORB organized lipid complex. Clin Cancer Res 2007;13:3079–3086. doi:10.1158/1078-0432.CCR-06-1889. [PubMed: 17505011]
40. Kadara H, Tahara E, Kim HJ, Lotan D, Myers J, Lotan R. Involvement of Rac in fenretinide-induced apoptosis. Cancer Res 2008;68:4416–4423. doi:10.1158/0008-5472.CAN-08-0031. [PubMed: 18519704]
41. Litvinov JVGDIV, Xu Y, Antony L, Dalrymple SL, Isaacs JT. Low-calcium serum-free defined medium selects for growth of normal prostatic epithelial stem cells. Cancer Res 2006;66:8598–8607. doi:10.1158/0008-5472.CAN-06-1228. [PubMed: 16951173]

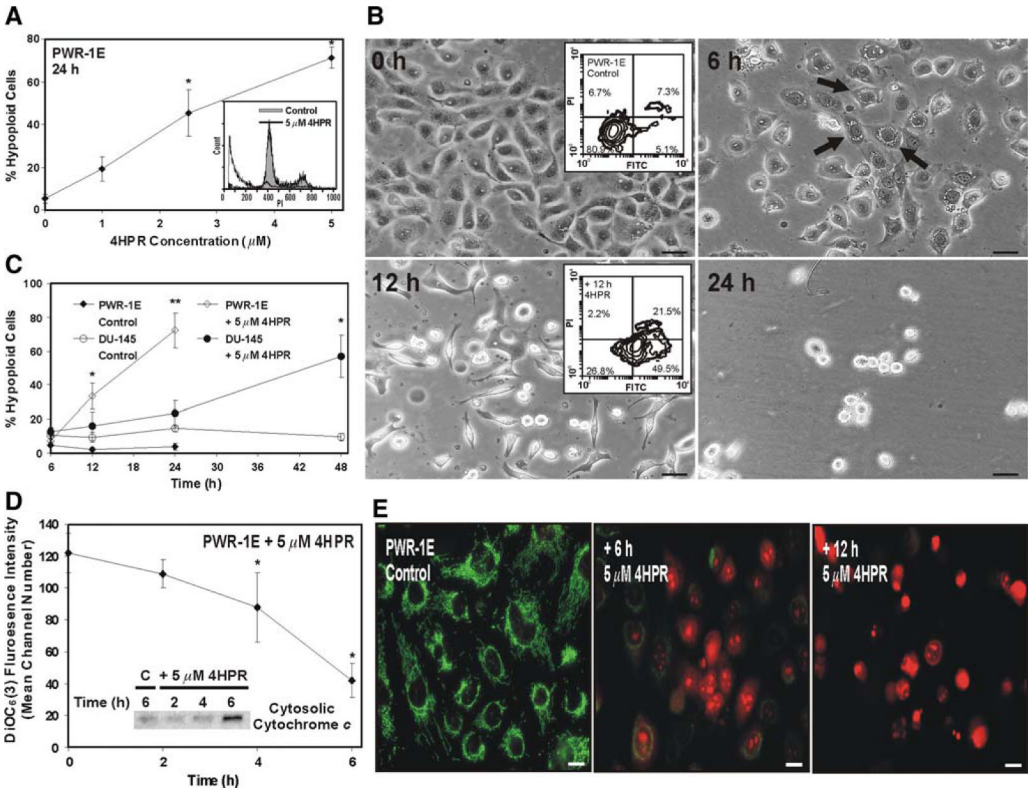

Fig. 1.

Evaluation of 4HPR-induced apoptosis in PWR-1E and DU-145 cells. **a** PWR-1E cells were treated with the indicated concentrations of 4HPR or an equal volume of the vehicle Me_2SO (0 μM 4HPR, control) and examined after 24 h for DNA degradation (% hypoploid cells) characteristic of apoptosis using hypotonic PI staining. The hypoploid cells have less cellular DNA content than cells typically found in the G_0/G_1, S, or G_2/M phases of the cell cycle, which causes them to retain less PI, a fluorescent DNA stain. The decreased retention of PI by the hypoploid cells shifts their fluorescence intensity leftward [i.e., cells detected below ~300 fluorescence units of PI on the linear *x*-axis of the representative histograms (*inset*)]. The results are expressed as a percentage of the mean hypoploid cells detected in triplicate samples for each treatment ± SD (*error bars*) (* $P < 0.01$ compared to control). **b** PWR-1E cells were photographed at the indicated times following exposure to 5 μM 4HPR. The floating cells and cell fragments are not seen in the photographs because the culture medium was removed prior to imaging. The cultures were imaged using a Nikon microscope and digital camera. The *scale bars* equal 36 μm. The PWR-1E cells with pearly cytoplasmic vacuolizations are indicated with arrows. The *insets* show the appraisal of cell membrane phosphatidylserine externalization in PWR-1E treated for 12 h with 5 μM 4HPR or the vehicle Me_2SO (control). Phosphatidylserine (indicated by the increase in FITC fluorescence intensity) was detected with annexin V-conjugated FITC. PI exclusion was used to illustrate plasma membrane integrity. **c** PWR-1E and DU-145 cells were treated for the indicated times with Me_2SO (control) or 5 μM 4HPR and examined for apoptosis using hypotonic PI staining as described above. The results are expressed as a percentage of the mean hypoploid cells detected in triplicate samples for each treatment ± SD (*error bars*) (* $P < 0.01$ compared to the appropriate 12- or 48-h control, ** $P < 0.001$ compared to control). **d** PWR-1E cells were exposed for the indicated times to 5 μM 4HPR or an equal volume of the vehicle Me_2SO (time 0). The $\Delta\Psi_m$ was determined by staining with $DiOC_6(3)$ and cytofluorometric analysis. The results are expressed as the mean of triplicate samples for each treatment ± SD (*error bars*) (* $P < 0.01$

compared to the vehicle Me_2SO). The inset shows an immunoblot assessment of cytosolic cytochrome *c* in permeabilized PWR-1E cells following exposure to 5 μM 4HPR or an equal volume of the vehicle Me_2SO (control, C) for the indicated times. **e** PWR-1E cells were treated for 6 h with Me_2SO (control) or 6 or 12 h with 5 μM 4HPR. After treatment, the cells were stained with 40 nM $DiOC_6(3)$ and 5 μM dihydroethidium as describe in the Materials and Methods and imaged via a Nikon epifluorescence microscope. The *scale bars* equal 16 μm

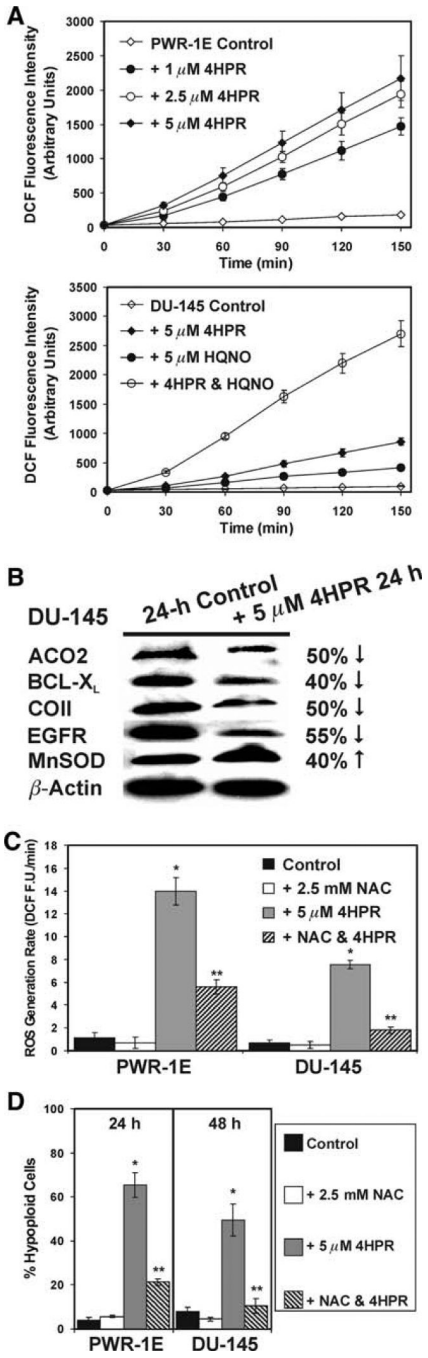

Fig. 2.

4HPR functions as a prooxidant in PWR-1E and DU-145 cells. **a** PWR-1E cells were exposed for the indicated times to 1, 2.5, or 5 μM 4HPR or an equal volume of the vehicle Me_2SO (control), and examined for the oxidation of 2′,7′-dichlorofluorescin to DCF using a microplate spectrofluorimeter. The assay described above was repeated using DU-145 cells exposed Me_2SO (control), 5 μM 4HPR, 5 μM HQNO, or 4HPR and HQNO. The spectrofluorimeter preformed 12 fluorescence measurements per well and calculated the mean value. Triplicate wells for each sample were measured. **b** Immunoblot analysis of cellular proteins in DU-145 cells exposed for 24 h to Me_2SO (control) or 5 μM 4HPR. The antibodies included mitochondrial aconitase (*ACO2*), BCL-X_L, cytochrome *c* oxidase subunit II (*COII*), epidermal

growth factor receptor (*EGFR*), Mn superoxide dismutase (*MnSOD*), and the loading control *β*-actin. The band intensity was normalized as a percent of the loading control *β*-actin using ImageJ software, and the percent decrease or increase of the examined proteins in the 4HPR-treated cells was measured relative to the same proteins in the control cells. **c** PWR-1E and DU-145 cells were pretreated for 2 h with 2.5 mM NAC followed by a 2.5 h exposure to 5 μM 4HPR or an equal volume of the vehicle Me_2SO (control). The cells were examined for the oxidation of 2′,7′-dichlorofluorescin to DCF using a microplate spectrofluorimeter as described in **a**. ROS generation rates (fluorescence units/min, FU/min) were derived from the slopes of lines obtained between 30 and 120 min from triplicate wells in 6-well tissue culture plates. The results are expressed as the mean of triplicate samples for each treatment ± SD (*error bars*)(* $P < 0.001$ compared to control, ** $P < 0.01$ compared to 4HPR). **d** The PWR-1E and DU-145 cells were assessed for hypoploid cells by cytofluorometric analysis as described in Fig. 1a after a 2-h pretreatment with NAC followed by a 24-h (PWR-1E) or 48-h (DU-145) exposure to the vehicle Me_2SO (control) or 4HPR. The results are expressed as the mean of triplicate samples for each treatment ± SD (*error bars*) (* $P < 0.001$ compared to control, ** $P < 0.001$ compared to 4HPR)

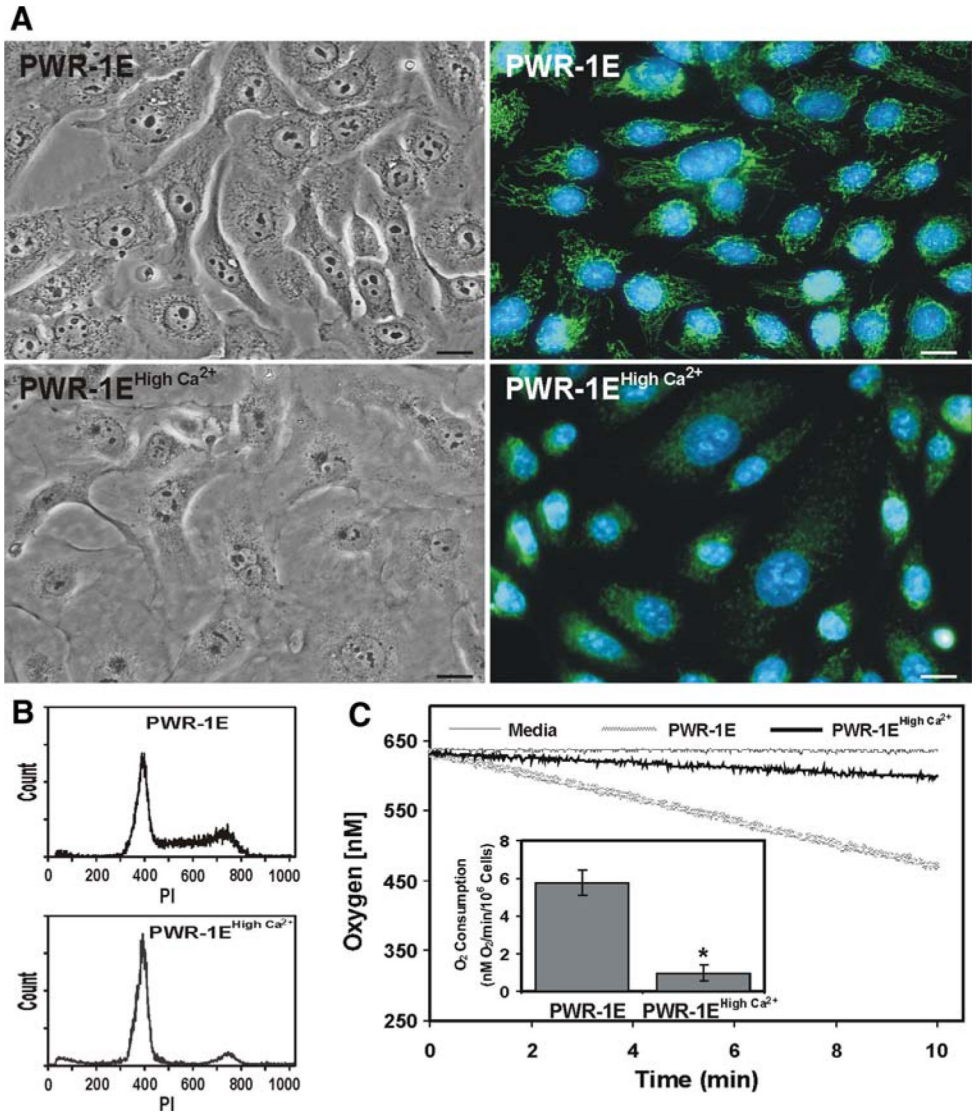

Fig. 3.

Ca^{2+} induces morphological, cell cycle, and bioenergetic changes in PWR-1E cells. **a** PWR-1E cells were cultured in KGM or KGM with 1.9 mM Ca^{2+} (i.e., PWR-1E high Ca^{2+}) for 6 days. The cells were imaged using light and epifluorescence microscopy. For the epifluorescence images, the cells were stained with 40 nM $DiOC_6(3)$ to visualize the mitochondrial network and 5 μg/ml of Hoechst 33342 to visualize the cell nucleus. The *scale bars* equal 18 μm. **b** Cell cycle distributions for the cells cultured as described in A were determined using hypotonic PI staining and flow cytometry as described in Fig. 1a. **c** Plots of O_2 consumption in PWR-1E cells cultured in KGM or KGM with 1.9 mM Ca^{2+} (i.e., PWR-1E high Ca^{2+}) for 6 days as described in **a**. A media blank served as a negative control for O_2 consumption. The O_2 consumption results depicted in the inset graph are normalized for 10^6 cells and expressed as the mean of triplicate samples for each treatment ± SD (*error bars*) (* $P < 0.001$ compared to the PWR-1E cells cultured under the normal low Ca^{2+} conditions)

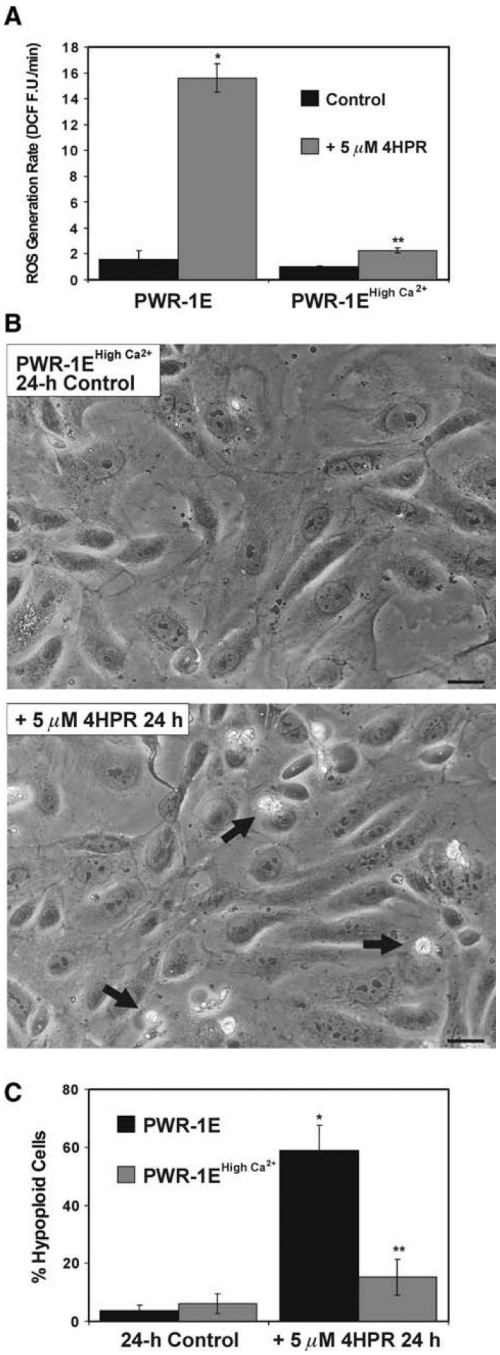

Fig. 4.

PWR-1E cells cultured in high Ca^{2+} KGM exhibit reduced sensitivity to 4HPR-induced ROS and apoptosis. **a** PWR-1E cells were cultured in 6-well tissue culture plates as described in Fig. 2a. The cells were exposed for 2.5 h to 5 μM 4HPR or an equal volume of the vehicle Me_2SO (control), and examined for the oxidation of 2′,7′-dichlorofluorescin to DCF using a microplate spectrofluorimeter. ROS generation rates (fluorescence units/min, FU/min) were derived from the slopes of lines obtained between 30 and 120 min from triplicate wells in 6-well tissue culture plates. The results are expressed as the mean of triplicate samples for each treatment ± SD (*error bars*)(* $P < 0.001$ PWR-1E cells cultured in KGM and treated with 4HPR compared to their control, ** $P < 0.01$ compared to the PWR-1E cells cultured in KGM

and treated with 4HPR). **b** Images showing PWR-1E cells cultured in KGM with 1.9 mM Ca^{2+} (i.e., PWR-1E high Ca^{2+}) exposed to Me_2SO (control) or 5 μM 4HPR for 24 h. The remnants of apoptotic cells in the 4HPR-treated culture are indicated with arrows. The floating cells are not seen in the photographs because the culture medium was removed prior to imaging. The *scale bars* equal 18 μm. **c** A summary of the hypoploid DNA content for cells examined in the experiments described in **b**. The results are expressed as a percentage of the mean hypoploid cells detected in triplicate samples for each treatment ± SD (*error bars*) (* $P < 0.001$ PWR-1E cells cultured in KGM and treated with 4HPR compared to their control, ** $P < 0.01$ compared to the PWR-1E cells cultured in KGM and treated with 4HPR)

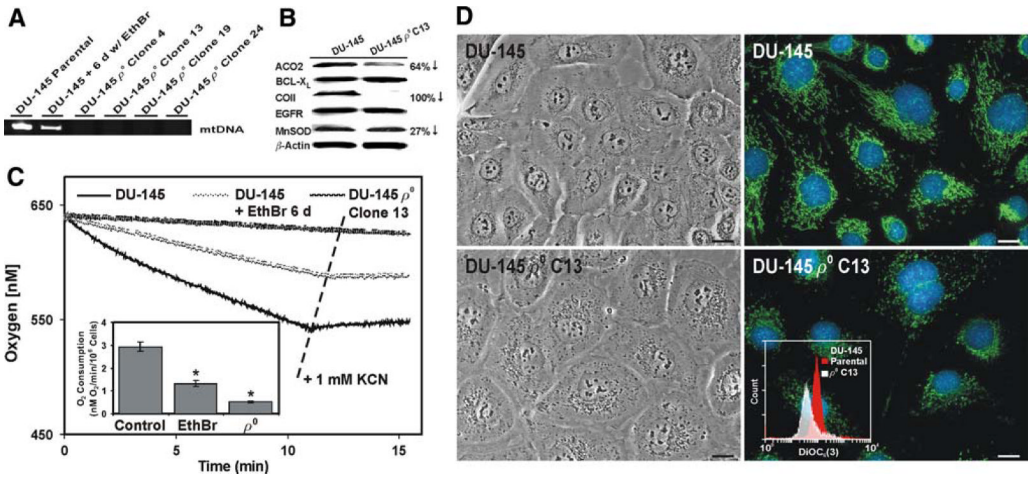

Fig. 5.

Characterization of the DU-145 ρ^0 cells. **a** DU-145 cells were exposed to medium containing 100 ng/ml EthBr for 6 days or 8 weeks and examined for mtDNA sequences using a PCR assay. **b** Immunoblot examination of protein levels in the parental DU-145 cells and the DU-145 ρ^0 clone 13. The antibodies included mitochondrial aconitase (*ACO2*), BCL-X_L, cytochrome *c* oxidase subunit II (*COII*), epidermal growth factor receptor (*EGFR*), Mn superoxide dismutase (*MnSOD*), and the loading control β-actin. The band intensity and relative protein levels were determined as described in Fig. 2b. c Plots of O_2 consumption in the parental DU-145 cells, DU-145 cells cultured for 6 days in medium containing EthBr, or the DU-145 ρ^0 clone 13 cells. Where indicated, KCN (a final concentration of 1 mM) was added directly to the respiration chamber using a syringe. The O_2 consumption results depicted in the inset graph were normalized for 10^6 cells and expressed as the mean of triplicate samples for each treatment ± SD (*error bars*) (* $P < 0.01$ compared to the parental DU-145 cells). **d** The parental DU-145 cells and the DU-145 ρ^0 clone 13 cells were imaged using light and epifluorescence microscopy. For the epifluorescence images, the cells were stained as described in Fig. 3a. The *scale bars* equal 18 μm. The inset graph shows the $DiOC_6(3)$ staining for 2×10^6 DU-145 and the DU-145 ρ^0 clone 13 cells analyzed via flow cytometry as described in Fig. 1d

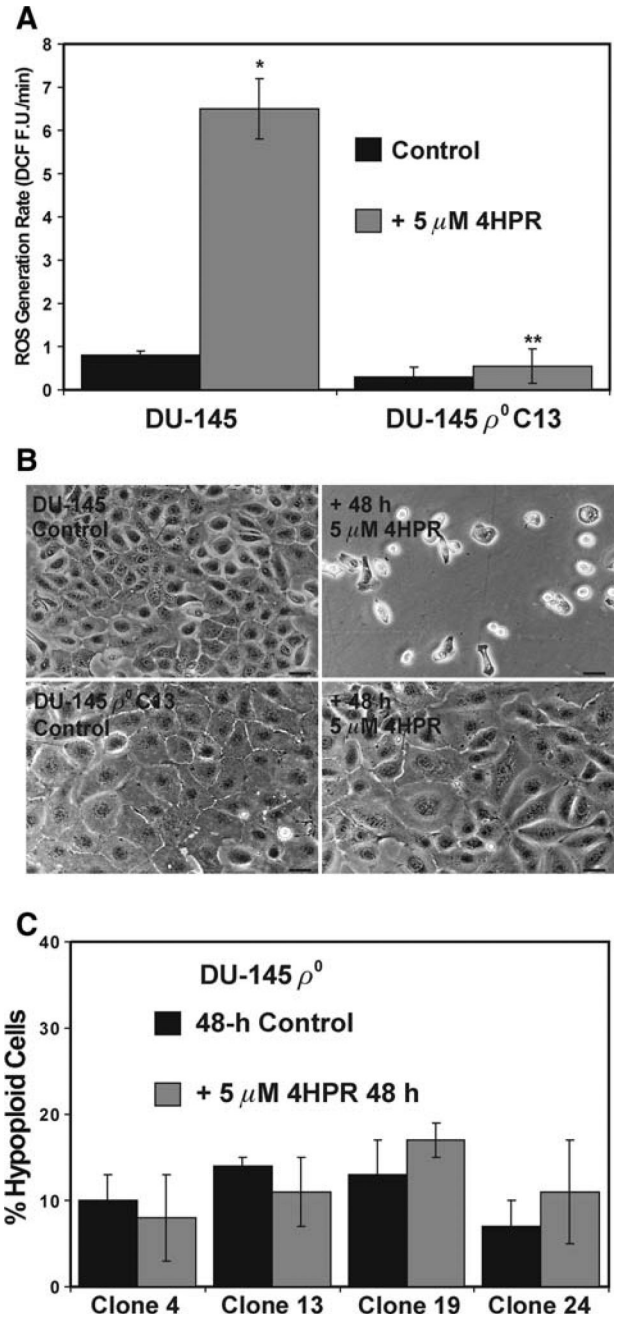

Fig. 6.

DU-145 ρ^0 cells are markedly resistant to 4HPR-induced ROS production and apoptosis. **a** The parental DU-145 cells and the DU-145 ρ^0 clone 13 cells were examined ROS generation as described in Fig. 4a. The results are expressed as the mean of triplicate samples for each treatment ± SD (*error bars*) (* $P < 0.001$ compared to the parental control, ** $P < 0.001$ compared to the parental DU-145 cells treated with 4HPR). **b** The parental DU-145 cells and the DU-145 ρ^0 clone 13 cells were treated for 48 h with 5 μM 4HPR or an equal volume of the vehicle Me_2SO (control). The cultures were imaged using a Nikon microscope and digital camera. The *scale bars* equal 36 mm. **c** As described in Fig. 1a, the amount of hypoploid cells was assessed using hypotonic PI staining in four of the DU-145 ρ^0 derivatives following a 48-

h exposure to 5 μM 4HPR or Me_2SO (control). The data are expressed as the mean of triplicate samples ± SD (*error bars*)

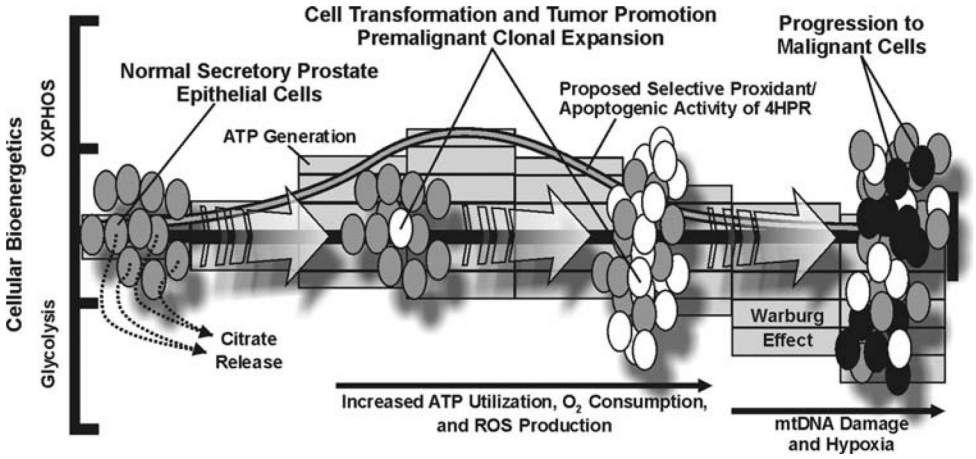

Fig. 7.

A diagram illustrating a prospective mechanistic basis for 4HPR-induced ROS and apoptosis in transformed prostate epithelial cells. Please see the text of the introduction and discussion for details